

Article

## Evidence of a Biological Control over Origin, Growth and End of the Calcite Prisms in the Shells of *Pinctada margaritifera* (Pelecypod, Pterioidea)

Jean-Pierre Cuif <sup>1,\*</sup>, Manfred Burghammer <sup>2</sup>, Virginie Chamard <sup>3</sup>, Yannicke Dauphin <sup>1</sup>, Pierre Godard <sup>3</sup>, Gilles Le Moullac <sup>4</sup>, Gernot Nehrke <sup>5</sup> and Alberto Perez-Huerta <sup>6</sup>

1 Department of Earth Sciences, Paris-Sud University, Bt. 504, 91405 Orsay, France;

E-Mail: yannicke.dauphin@u-psud.fr

2 Department of Analytical Chemistry, Gent University, Krijgslaan 281 S12, 9000 Gent, Belgium;

E-Mail: burgham@esrf.fr

3 Institut Fresnel UMR 7249, Aix-Marseille University, Centrale Marseille, 13013 Marseille, France;

E-Mails: virginie.chamard@fresnel.fr (V.C.); pierre.godard@univ-poitiers.fr (P.G.)

4 Ecosystèmes insulaires océaniques UMR 241, Institut français de recherche pour l'exploitation de la mer (IFREMER) Centre du Pacifique, 98719 Taravao, Tahiti, French Polynesia;

E-Mail: gilles.le.moullac@ifremer.fr

5 Alfred Wegener Institute for Polar and Marine Research, Am Handelshafen 12, 27570 Bremerhaven, Germany; E-Mail: gernot.nehrke@awi.de

6 Department of Geological Sciences, The University of Alabama, 2018 Beville Building, Tuscaloosa, AL 35487, USA; E-Mail: aphuerta@as.ua.edu

\* Author to whom correspondence should be addressed; E-Mail: jean-pierre.cuif@u-psud.fr; Tel.: +33-016-915-6741.

External Editor: Kota Hanumantha Rao

Received: 13 October 2014; in revised form: 18 November 2014 / Accepted: 10 December 2014 /

Published: 18 December 2014

---

**Abstract:** Consistently classified among the references for calcite simple prisms, the microstructural units that form the outer layer of the *Pinctada margaritifera* have been investigated through a series of morphological, crystallographical and biochemical characterizations. It is often said that the polygonal transverse shape of the prisms result from the competition for space between adjacent crystals. In contrast to this classical scheme the *Pinctada* prisms appear to be composed of four successive developmental stages from the concentrically growing disks on the internal side of the periostracum to the

morphological, structural and compositional changes in both envelopes and mineral components at the end of the prisms. These latest structural and compositional changes predate nacre deposition, so that the end of prism growth is not caused by occurrence of nacre, but by metabolic changes in the secretory epithelium. This sequence makes obvious the permanent biological control exerted by the outer cell layer of the mantle in both organic envelopes and mineralizing organic phases.

**Keywords:** biomineralization; bivalve shell; microstructure; calcite prisms

---

## 1. Introduction

Shells of *Pinctada margaritifera*, the bivalve species on which Polynesian pearl industry relies, exhibit simple organization and structure. The marginal area of the mantle produces the outer shell layer, constructed from densely packed calcite prisms perpendicular to shell surface, whereas the internal regions of the mantle produce nacre, the “mother of pearls” composed of aragonite tablets. The scaly aspect of the external surface of the shell result from an alternating backwards and forwards directional growth process resulting in an increase in the overall size of the shell, with the nacre progressively covering the internal surface of the outer prismatic layer (Figure 1a,b: arrows).

In addition to the nacreous material that has triggered extensive economic interest and continued investigation during the last century [1], the calcite prisms that form the outer shell layer in *Pinctada* (and members of *Pteriidae* family) have also drawn attention owing to their easily visible structural patterns. These prisms were invariably classified as “simple prisms” in the main treatises describing structural organizations of Mollusk shells [2–6]. Their overall characteristics (Figure 1c–e) observed at the growing edges of young shells justify such a classification. Prisms appear as well defined units whose limits are marked by a polygonal organic network that can be made visible by light acidic etching (Figure 1c), and strongly emphasized by its fluorescent response to green laser light (Figure 1d). When thin sections are observed between crossed-nicols (polarizing microscope), each mineral component within the organic honeycomb structure exhibits a single-crystal optical behavior (Figure 1e). Therefore question arises regarding the determinism of a crystallization process that enables formation of such regular crystal-like units without any known precursor.

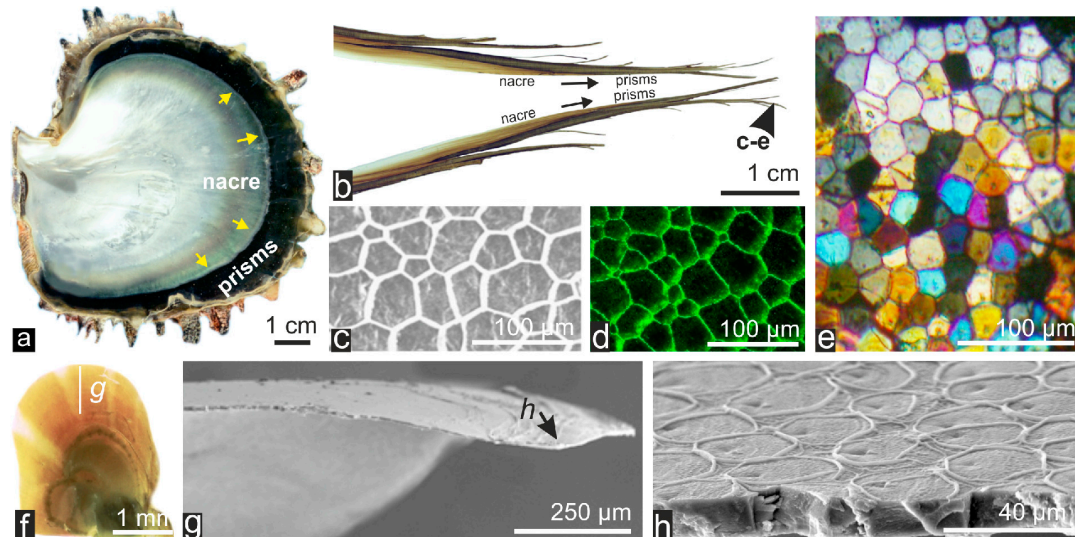
Earlier investigators considered that the organic components present at the distal crystallization site (*i.e.*, the internal side of the periostracum) played only a passive role in the formation of the polygonal pattern of the prism envelopes. Wilbur (Figure 10 in [7]) for instance, commenting on microscopic data from Wada (Figure 8 in [8] (p. 780); see also this paper Figure 8b) observed circular crystalline units growing “in oolitic aggregation” becoming progressively polygonal by mutual contact. Wilbur [7] (p. 161) wrote: “The organic matrix, displaced by the growing crystals surrounds and separates the individual crystals as they grow together”. In this scheme, the prism envelopes appear to be constructed from residual organic matrix, which “finally hardens”. A comparable view was proposed by Taylor and Kennedy [9]: “It is suggested that calcium carbonate deposition begins so close to the margin that not all the protein forming the inner layer of the periostracum has polymerized from the extrapallial fluid by the

time calcium carbonate precipitation begins. The periostracum ingredients cannot be incorporated into the crystal structure and are squeezed out as impurities to the edges of the growing crystals”.

In such views, formation of the polygonal network commonly referred to as “prism envelopes” appears as an essentially passive process, a sort of by-product of the crystallization process itself. Note must be made that no information is provided regarding the long reported overall similarity in crystalline orientation of the prisms where statistically the *c* axes are perpendicular to the shell surface, and no attention is paid to the absence of regularity in the transversal sections of the similarly oriented crystalline units. The competitive crystal growth has been postulated for the polygonal section of the prisms: growing crystals compete for space with adjacent crystals.

In contrast to this concept of a simultaneous formation of the prismatic crystalline units and their surrounding organic polygons, Mikkelsen *et al.* (Figure 17 in [10]) described a series of rings “varying in shape and size, not closely adjacent to one another” located on the outer surface of the shell margin of the *Pinctada longisquamosa* (from Florida Keys, FL, USA). This appears to be the first mention of a structural stage predating the polygonal status of the shell outer layer. Figure 1f–h shows that a similar ring pattern is present on the outer surfaces of the shell of *Pinctada margaritifera*.

**Figure 1.** Structure of the shell and prismatic shell outer layer from adult and juvenile *Pinctada*. (a, b): Typical prismatic-nacreous sequence; (c–e): Organic envelope (c, d) and single crystal-like pattern of the calcite prisms (e); (f–h): Juvenile shells (f) showing the ring pattern on the outer surface of the prismatic layer (g, h).

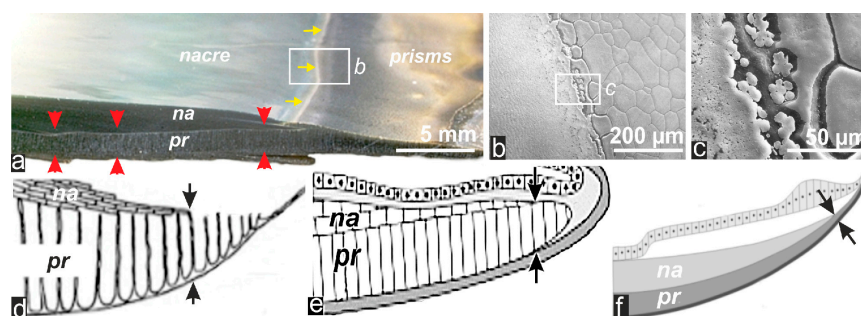


Employing juvenile *P. margaritifera* shells, the origin of these rings have been investigated, and the role of the corresponding mineral components produced during the early mineralization sequence predating the prismatic polygons at the growing margin of the shells was recognized.

At the opposite end of the prismatic units, on the internal side of the shell, it is generally accepted that the inward growth of the prisms is interrupted by spreading of the nacreous layer onto the internal prism surfaces. Such interpretation is supported by the simple observation of radial sections of shell perpendicular to the valve surface (Figure 2a) and details of the line marking the onward progression of the aragonite mineralizing area (Figure 2b,c). On the other hand, worth to note that from recent literature questions remain about the overall growth process of the prisms: several authors seemingly admit their

ability to grow after having been covered by nacre (Figure 2d–f), leaving unexplained the mechanism allowing for such a phenomenon.

**Figure 2.** Growing area of a *P. margaritifera* shell and schemes of prism elongation posterior to nacre deposition. (a): Radial section showing both the progression of the calcite prisms into the nacreous layer (yellow arrows) and the fixed thickness of the prismatic layers once covered by the nacre (red arrows); (b, c): Closer view of the transition between the calcite and aragonite areas. Note the precise arrangement of the first aragonite patches onto the organic lamella covering the prism surface; (d–f): Examples of published schemes showing the prolonged growth of the prisms after coverage of their inner surface by nacre (d: from [11]; e: from [12]; f: from [13], redrawn.)



This paper brings together a range of structural and biochemical data provided by physical characterizations of the structures observed between origin and end of the prisms, prior to coverage of their internal surface by the nacreous layer. This sequence of distinct mineralization events suggests a permanent control exerted by the mineralizing cell layer of the mantle on the microstructural patterns of the prisms of the *Pinctada margaritifera*, in contrast with the current concept still largely influenced by chemical crystallization mechanisms.

## 2. Results: The Sequential Growth of the Prisms from Their Early Stage to Their End

Four distinct developmental stages can be characterized between the early beginning of the prisms and the end of their growth:

- (1) Formation of initial calcite disks as isolated and separately growing units;
- (2) First prismatic stage exhibiting a single crystal-like behavior and a synchronous layered thickening;
- (3) Passage to a polycrystalline prismatic structure;
- (4) Progressive degradation of the mineralizing metabolism and final coverage of the prism growing surface by a specifically secreted organic layer, on which aragonite deposition commences.

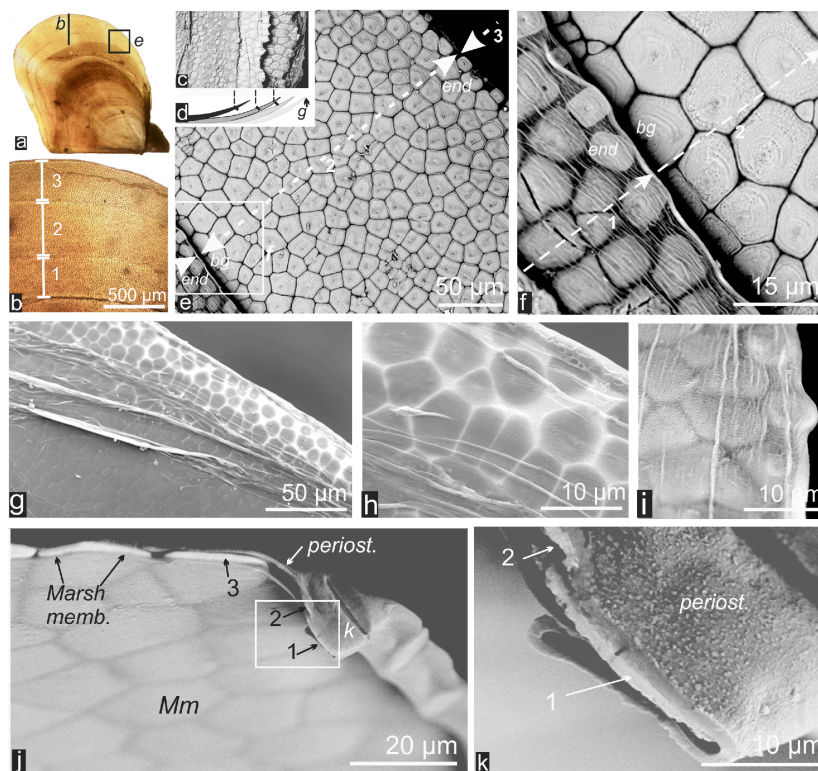
### 2.1. Formation of Calcareous Disks at the Shell Growth Margin: The Initial Stage in Calcification of the Prismatic Layer

The foremost-mineralized components of the shell valve appear as isolated, flat and approximately circular units that are most easily visible in young shells at the outer margin of every growth phase. The alternating backwards and forwards directional growth process that produces the scaly morphology of the adult *Pinctada* shell is already present in the youngest post-metamorphosis shells. Figure 3a–f

illustrate this mode of growth as seen from the outer surface of the young shell, characterized by the repeated production of growth lamellae whose development is limited in time (Figure 3a,b).

During this process, the marginal structures of the growth lamellae are repeatedly broken due to the backward displacement of the mantle at the end of each growth period (retraction) and the consecutive rupture of the periostracum (Figure 3c,d). As a result it is noteworthy that in a given shell, description of the very initial calcified structures is possible only from the last growth lamella, details about the earliest calcification stages relying on structures whose further growth has been interrupted at the end of the last growth cycle (Figure 3g–i).

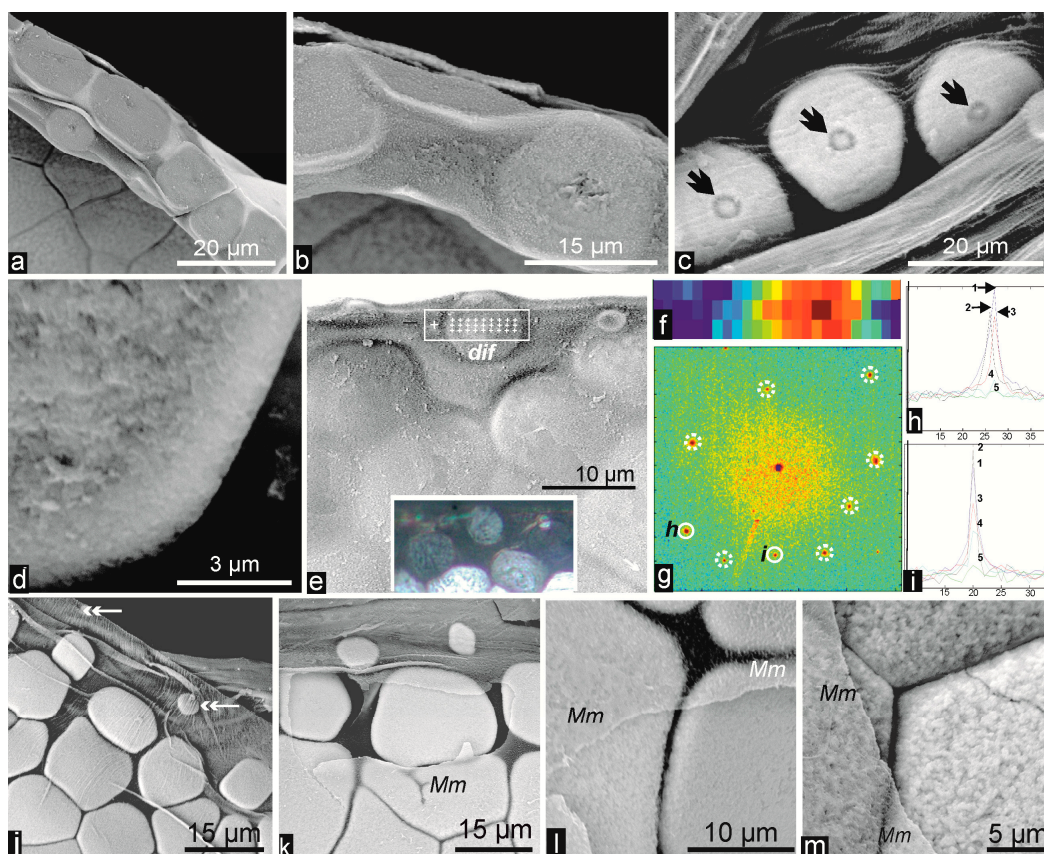
**Figure 3.** Stepping elongation of the shells and discoid units formed at the marginal growth area. (a–d): Examples of the sequential growth based on a succession of lamellar growth stages (a, b) repeatedly inserted onto the internal side of the previous growth stage (c, d); (e, f): Overall view of a growth stage (e) and detail (f) of the contact between the end of the previous growth stage (1) and the beginning of the subsequent stage (2): note the morphological changes between the polygonal structures produced at the beginning of the growth (bg) and those of the end. A continuous line marks the insertion of the recent lamella onto the last elements of the previous growth unit (arrow); (g–i): Discoid units at the margin of a growth lamella, visible below the periostracum; (j–k): Visible in this profile view of a fractured shell, the discoid units are sandwiched between the periostracum (outer surface) and the Marsh membrane (Mm) on the inner side of the shell.



In Figure 3j,k the first rank mineralized structures can be seen distinctly (see also Figure 4a–c): they are sandwiched between the periostracum and the inner organic Marsh membrane [14]. In favorable cases, the circular units growing separately at the lamella margin have been made visible by the preparative process, and are clearly exposed due to the periostracum folding (Figure 4). The disks are

flattened, approximately 1.5 micrometer thick and up to 15–18 micrometers in diameter (Figure 4a–c). The existence of an initial centre is sometimes visible (Figure 4b,c) surrounded by concentric mineralization, but this pattern is usually masked by further calcification.

**Figure 4.** Structure and crystallography of the discoid mineral units at the shell growth margin. (a–c): Periostracum folding enables a series of flat and separately growing disks to be visible, revealing their initial centers (arrows); (d): Rough surface and granular periphery of the disks; (e): A series of X-ray Bragg diffraction was carried out on a single disk whose observation between crossed nicols suggests a single crystal-like structure (insert); (f–i): X-ray microdiffraction data confirm an overall single crystal-like behavior for the disks: integration of the diffraction Bragg peaks from the 27 disk sites are illustrated as both Bragg peaks diagrams in the detection plane (g) and angular orientation exemplified by two distinct spots and peaks (h, i); (j–m): Mineralized disks viewed from the inner side of shell valve: note the well visible Marsh membrane (Mm), the granularity of the mineralized structure (l, m) and the absence of organic envelopes surrounding the disks even when they are in contact at the end of their lateral growth.

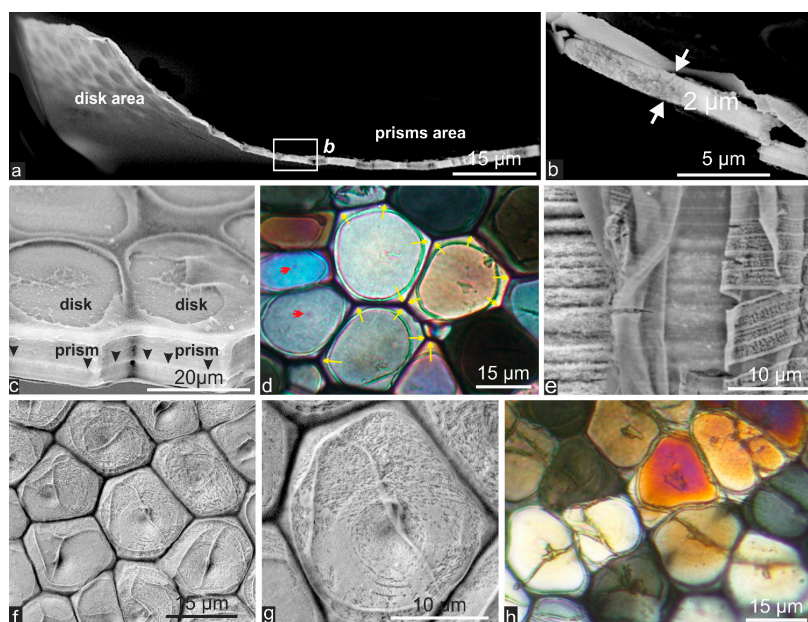


The mineral surface has a distinctive granular appearance visible on partly isolated disks (Figure 4d). In spite of the granular appearance these discoid units appear to be well crystalline. This can be formally established through a series of X-ray micro-diffractions where the sub-micron beam spot is scanned through three parallel series of nine points resulting in 27 distinct diffraction measurements (Figure 4e: *dif*) within a single disk (with steps of  $2 \times 1 \mu\text{m}^2$ ). The individual Bragg peaks integrated spatially across the disk produces well-defined and isolated Bragg spots (Figure 4g–i). These

demonstrate the overall crystalline consistency of the disk, resulting in a single crystal-like behaviour at the resolution of the optical microscope in spite of morphological evidence of a concentric growth mode.

It should be noted that the opposite surface of the disks (= internal side) has a distinct appearance. Taking advantage of the irregular folding of the periostracum, the morphological changes of the mineralized units located onto its internal surface are well exposed (Figure 4j,k). Closer observation through the transparent Marsh membrane reveals that the internal surface is also finely granular (Figure 4l,m). In addition, these two last figures reveal that no membrane exists between the mineralized units: even when having reached a polygonal morphology they are very close to each other (Figure 4m). Profile views (Figure 5a,b) confirm that growth of these early skeletal components is essentially lateral: their thickness remains in the micrometer range from their very early growth stages (when they are very distant), to their final stages when they are practically in contact.

**Figure 5.** From individually growing disks to layered mineralization of prisms. **(a, b)**: Lateral view of a fractured juvenile *Pinctada* shell showing sections of the about 2 micron thick disks; **(c)**: View of the round shaped limits of the disks still visible at the outer surface of the early stages of the prisms. Arrows underline their common layered growth mode, fully distinct from the individual growth mode of the disks; **(d)**: Transmitted polarized light view of the early prismatic layer (crossed nicols). Note that the mineral phase of the prisms oversteps the dimension of the disks (arrows); **(e)**: The organic network (envelopes) shows a stepping growth mode corresponding to layering of the mineral phase; **(f–h)**: Examples of sectors in which the newly formed organic network includes at least two mineral units produced during the initial stages.



## 2.2. Passage from Laterally Growing Disks to the Layered Growth Mode of the Prisms

The main structural difference between the two first stages in prismatic layer formation can be seen from the transverse section of the growing area of a young shell (Figure 5a–c). On the internal side of first stage units (whose maximal thickness is about two micrometers, see Figure 5b), a new mode of

mineral deposition occurs, characterized by synchronism of the mineral layers between adjacent units (Figure 5c: arrows). Traces of the early disks are readily visible as remnants of the initial stages (Figure 5c). Observation of this developmental stage between cross-nicols (Figure 5d) clearly shows that formation of the polygonal prisms occurs at this stage only: the polygonal crystal-like units overstep the circular limits of the disks. Formation of the polygonal organic network (envelopes) also occurs at this stage: its stepping growth mode strictly corresponds to layering of the mineral phase (Figure 5e). It frequently occurs that the polygonal units of the organic network include two or more of the smaller and irregular discoid units produced during the first mineralizing phase, as assessed by both microstructural and polarized light observations (Figure 5f–h). Such a stepping and coordinated production of both mineral and organic components results in the typical layered growth mode of the prisms [15].

### *2.3. Microstructural Change during Prism Growth: Passage from a Single-Crystal to Polycrystalline Microstructure*

Up to about 150  $\mu\text{m}$  in thickness, the layered biomineralization process maintains the initial crystal-like consistency of the prisms (Figure 6a–c), a status that abruptly changes with a remarkable synchronism between neighbor prisms. Observed from fractured surfaces perpendicular to shell plan, a modification in prism morphology can be seen (Figure 6d–f). Crystallization is also modified: instead of behaving as a single crystal, polarization and electron backscatter diffraction (EBSD) show that mineral phase of the prism (approximately 250  $\mu\text{m}$  long) is now subdivided into a variable number of parallel, but crystallographically distinct, subunits (Figure 6g,h). The limits between prism subunits are irregular during the course of their growth. Sections observed between crossed-nicols and polished-etched surfaces (Figure 6i,j) provide demonstrative images of this structural change.

Of note is that these crystalline subunits remain enclosed within the initial organic network (= envelopes) surrounding the previous single crystal-like prisms. Enzymatic etching has shown that subunits were separated by organic layers that were much more sensitive to enzymatic action than the firstly produced organic network [16] (Figure 2g,h). X-ray absorption near edge structure (XANES) mapping has also shown that limits between the crystalline subunits within a given prism are marked by reduced concentrations of sulfated polysaccharides (Figure 1j: arrows, in [16]).

### *2.4. Structural and Biochemical Changes Occurring at the Distal Growth Stages of the Prisms, Predating Nacre Deposition*

A series of structural and biochemical changes have been observed on polished longitudinal sections of the prisms (Figure 7a). Several tens of micrometers before the end of calcite deposition, the prism envelopes become irregularly thicker producing nodules visible through observation using UV fluorescence (Figure 7b) and more clearly with back scattered electron microscopy (Figure 7c). Infrared map also shows the patchy composition of the organic membranes between the aragonite and the prisms, and between the prisms (Figure 7d). Numerous holes observable in the envelope (Figure 7e,f) allow assessing the compositional changes among the organic components whose coalescence produces the polygonal organic network. Not only is envelope formation modified but changes also occur in composition of the organic components controlling calcite deposition. Reduction of growth layer thickness is the most apparent indication of this metabolic modification (Figure 7g). Moreover, before

deposition of the aragonite layer an organic film is formed that spreads onto the surface of the prism (Figure 7h, arrows). Biochemical composition of this prism-covering organic membrane has been shown to be distinct from that of prism envelopes [17]. It is confirmed by X-ray absorption mapping of magnesium and sulfur carried out at the specific energy for sulfur-bearing amino acids (Figure 7i,j). Of note is that such a consistent series of progressive alteration in formation of the calcite prisms occurs before aragonite deposition. It can be deposited as isolated patches (Figure 7k, arrows) whose subsequent junction to the prism envelopes completely isolates the calcite compartment. Importance of this prism-covering membrane is demonstrated by the precise localization of the very early aragonite patches that are only formed on this covering membrane (Figure 7k). Much frequently, continuation of the secretion of the prism-covering membrane is observed as irregular organic filaments incorporated in the aragonite domain (Figure 7b,c, arrows). That the prism closing membrane is an important component of shell development is shown by the sequential evolution of aragonite deposition, starting from the initial patches lying on the covering membrane, followed by fibrous aragonite and then by layered aragonite forming the nacreous tablets.

It is noteworthy that the microstructural sequence typical for the prism growth end is so deeply rooted in the overall mineralization metabolism of the *Pinctada margaritifera* that it is not confined to maturing oysters, but it can be recognized in the juvenile specimens aged only a few weeks (Figure 7l).

**Figure 6.** Coordinated change in prism structure: from single crystal-like to polycrystalline organization. (a, b): SEM Images of radial section (perpendicular to the shell plan) in the prismatic layer of a juvenile *Pinctada*; (c): Single crystal-like microstructure of the prisms (axial section) in a juvenile *Pinctada* (transmitted light, cross-nicols); (d–f): SEM images of the prisms showing the coordinated morphological changes; (g, h): Crystalline subunits of the prisms viewed in thin axial sections (g) and EBSD (h): Single crystal-like behavior is maintained in spite of the irregular limits of the subunits (credit picture: Sandra Piazzolo, unpublished); (i, j): Polycrystalline prisms in microscopic thin section (i): transmitted light crossed-nicols), and etched sections showing the sinuous etching-sensitive organic limits between prisms (j).

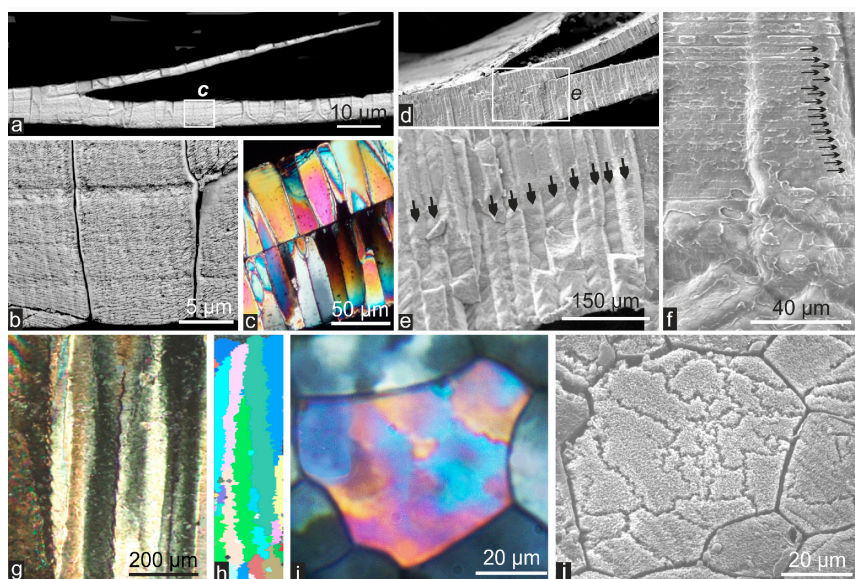
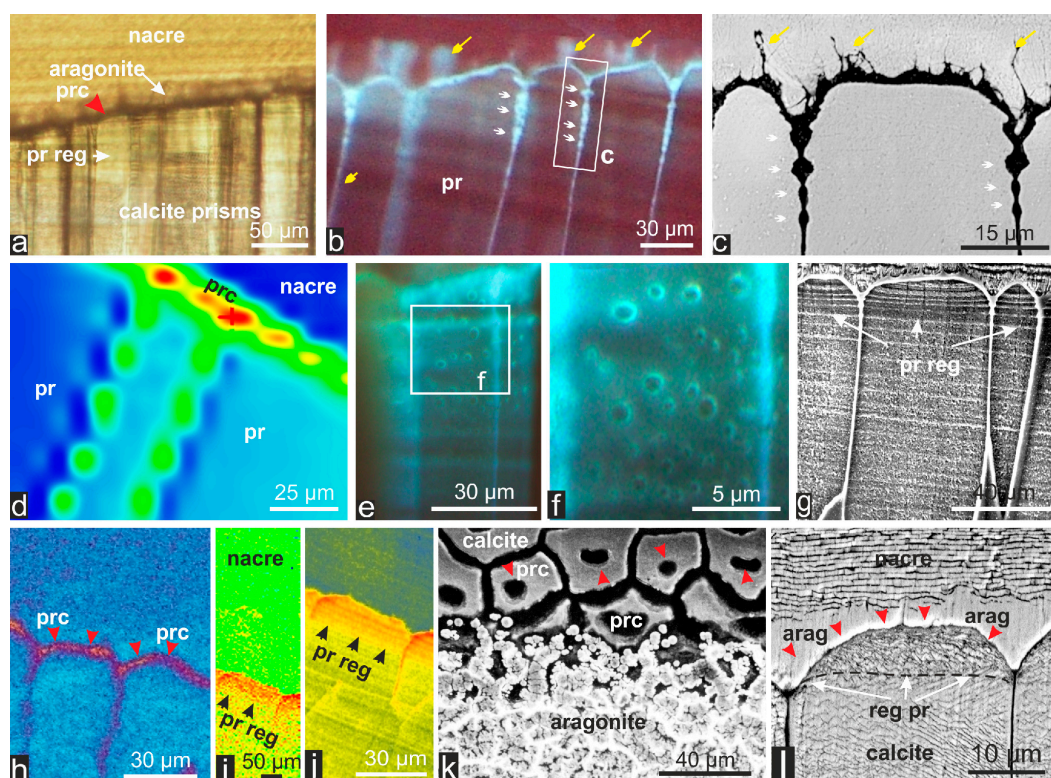


**Figure 7.** Evidence for a biologically controlled growth end of the prisms predating nacre deposition. **(a):** Microscopic thin section of the calcite/aragonite transition area: prism regression (pr reg, arrows) followed by deposition of the prism covering membrane (prc), then by aragonite materials; **(b):** UV fluorescence of an equivalent area. Note the morphological modification of the prism envelopes (arrows); **(c):** Back scattered electron (BSE) imaging of the same area, emphasizing the morphological changes of the prism envelopes and the filamentous continuation of the organic layer covering the prism (yellow arrows); **(d):** Infrared map at  $1565\text{ cm}^{-1}$  (amide II) showing the patchy composition of the organic envelopes surrounding the prisms and that of the organic membrane between the calcite and aragonite (prc); **(e, f):** Holes observed in the prism envelopes; **(g):** Reduction of growth layer thickness and restricted mineralizing areas provide morphological evidence of regression of prisms (pr reg); **(h):** Time-of-flight secondary ion mass spectrometry (TOF-SIMS) distribution map of alanine concentration in the prism covering membrane showing the specific composition of the prism covering film (credit picture [17]); **(i):** Distribution map of Mg showing the change in composition of the prisms before the deposit of the aragonite; **(j):** XANES map emphasizing compositional modification of sulfated part of the mineralizing matrices confirm metabolic changes in the mineralizing cells; **(k):** Patchy stage deposition of the prism covering organic membrane favoring aragonite deposition; **(l):** Transition calcite/aragonite observed in a juvenile *Pinctada* shell.



### 3. Discussion

This study shows that the calcite prisms of the *Pinctada margaritifera* are constructed employing a developmental sequence that can be incorporated into the overall scheme of shell formation as summarized by Taylor and Kennedy [9] (p. 275): “Evidence suggests that there is a generative zone in

the inner part of the periostracal groove and cells produced there change their form and function during the growth of the animal". What Taylor and Kennedy apply to the whole shell also fits perfectly with the structural history of the prismatic layer itself, as formation and developmental timing of the prismatic units are directly linked to the mechanism of shell growth at the outer margin of the mantle.

### 3.1. The Early Calcification Stages

According to Carter and Aller [18] and Carter [19], the periostracal mineralization mechanisms differ from those of the "adult" shell: the periostracal mineralization occurs on the "inner surface of the outer mantle fold, unlike calcification of the shell proper" in some taxa [18] (p. 317). In Mytilacea, the  $\text{CaCO}_3$  polymorph differs in the periostracal units and the underlying shell layer.

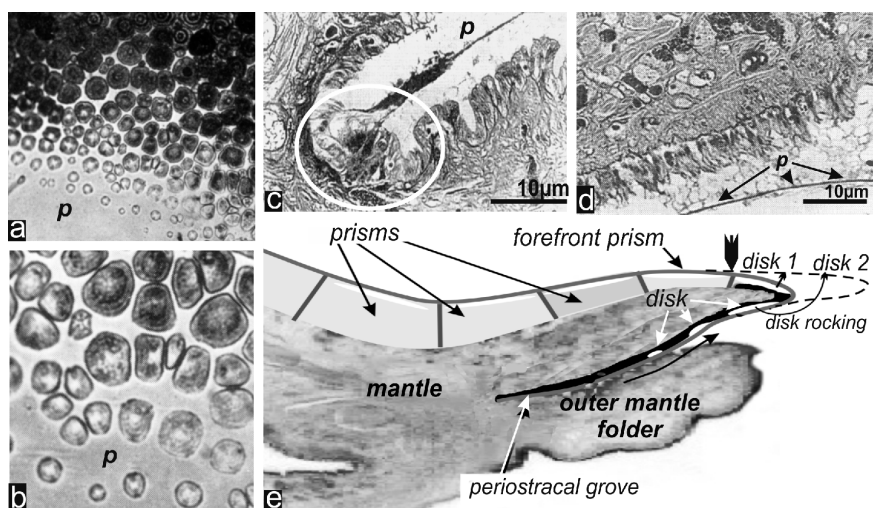
The growing disks pictured by Wada [8] and reproduced in Figure 8a,b illustrate the first stage of mineral deposition, and as stated by Taylor and Kennedy [9] (p. 275): "The first calcareous material is laid down from the epithelial cells of the outer fold (of the pallial margin)". Of note is that in the deeper part of the groove formed by this outer mantle folding, a group of specialized cells produces the periostracum (Figure 8c). Histological studies by Jabbour-Zahab *et al.* [20] have shown that cells of the epithelial groove secrete a layer of organic gel between their outer surface and the inner side of the periostracum (Figure 8d). Figure 8e summarizes the structural organization at the forefront of the growing shell and the overall trajectory of the disks during their development.

With respect to early deposition of calcite at the shell margin, two points need to be clarified relating to the data obtained by Wada. We employed optical microscopy (transmitted natural light) and diffractometric methods to establish the formation of calcite "with the periostracum" by Suzuki *et al.* [21]. Polarized-light microscopy and micro-diffraction experiments (Figure 4e–i) have confirmed that each of these rounded shaped units, whose diameters increase progressively during their transit in the outer mantle folder, exhibits a single crystal like pattern but at the same time they clearly grew concentrically around centers (Figure 9a). Regarding the origin of crystallization of the disks (and subsequent prism crystallinity), these spheroidal nodules (see also Figure 4a–c) show that, in addition to the secretion activity of the mantle groove epithelium (Figure 8d), the generative zone hypothesized by Taylor and Kennedy [9] also exerts a key role from a microstructural viewpoint. By distributing the organic globules acting as centers of crystallization within the organic layer secreted by the outer groove epithelium, the generative zone creates the structural framework which leads to formation of the disks, and finally the prismatic structure of the shell. From such a perspective, a striking correspondence can be established between these nodules responsible for prismatic microstructure of the shell outer layer, and the initial centers of the nacreous tablets observed by Nudelman *et al.* [22].

It is noteworthy that although the concentric growth pattern is visible at the surface of the disks (Figure 9a), this does not imply a fibro-radiating mode of crystallization as is usually associated with a centered organization. Atomic Force microscopy (AFM) observations reveal that mineral deposition occurs as parallel and densely packed rods (Figure 9d–g), themselves constructed by aligned grains of approximately 50–75 nanometres in mean diameter. As typical for calcareous biominerals, these grains are covered by an irregular cortex (Figure 9h). From Dauphin [23] up to Checa *et al.* [24], such a type of infra-micrometric organo-mineral structure has been recognized among various mollusk shell components and was extended to the skeletons of practically all other calcifying phyla [25]. Regarding

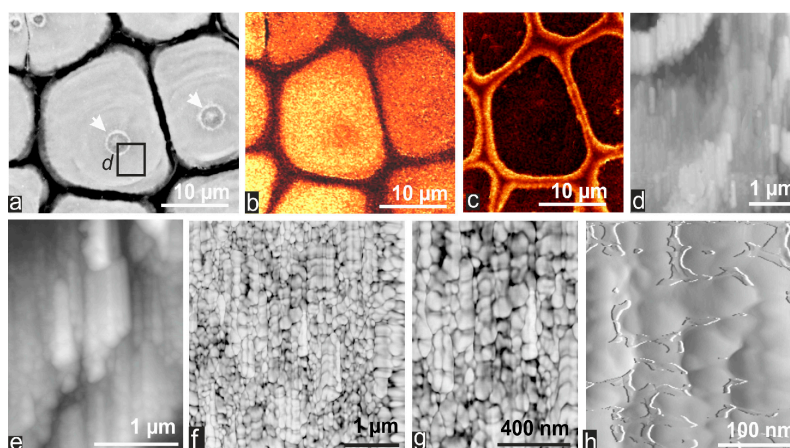
the *Pinctada*'s initial calcified structures it can be seen that overall orientation of the rods (themselves built by the submicrometric grains, Figure 9d–h) is consistent with the growth direction of the shell. Thus, infra-micrometric organization of the disks appears consistent with their macroscopic single crystal-like behavior, as observed in polarized light and detailed synchrotron based crystallographic characterization (Figure 4h,i). From a biomineralization viewpoint, consistency of rod orientation suggests a controlled crystallization that may be related to structural properties of the organic layer deposited onto the internal side of the periostracum. This oriented crystallization also deserves to be emphasized as a point of major importance regarding the next step in shell formation: the passage from disk to prism mode of growth.

**Figure 8.** Semi-schematic reconstruction of the sequential development of the shell growing edge. (a, b) Wada's [8] images of the rounded shaped units at the growth margin of the shell (natural transmitted light microscopy; p: periostracum). (c, d) Histological view of the deepest region of the periostracal groove, showing the periostracum producing area (c) and the organic deposition by the epithelial layer; (d) on the inner side of the periostracum (p) (modified from [20]). (e) Radial section of a *Pinctada* mantle margin showing the position of the growing disks (*disk*) within the organic gel underlying the outer side of the outer mantle folder. The scheme also indicates the next steps to occur when the more advanced disks (*disk 1* then *disk 2*) become aligned with the forefront prism through an almost 180° rocking movement, enabling their incorporation into the common layered growth mode of the shell. The black arrow marks this passage from the individual lateral growth mode typical of disks to the common thickening layered growth mode typical of prisms.



The final disk developmental stage implies a change in positioning of the disks to enable the most advanced ones to reach the appropriate location such in order to be in continuity to the shell plan (see Figure 8e). Activity of the cell generative zone of the periostracal groove epithelium (Taylor and Kennedy [9]), and concomitant secretion of the periostracum by the specialized cells (Figure 8b), lead to an extension of the tissue of the mantle groove, making possible the relevant change in orientation of the most advanced disks growing on the internal side of the periostracum (see also Griffin [26] who described this phenomenon at the *Nautilus* shell margin).

**Figure 9.** Infra-micrometric structure of the disks. (a): back scattered electron (BSE) image shows the concentric growth pattern of the disks around the central nodule; (b): Raman fluorescence imaging illustrating the distribution of calcite (calculated on the intensity distribution of the peak belonging to the symmetrical stretching of calcite  $\nu_1$  at  $1085\text{ cm}^{-1}$ ); (c): Imaging of carbon at the periphery of the disks. According to Chu and Li [27], this could be related to the remobilization of organics prior to formation of the mineral rods; (d–g): AFM height images (d, e) and phase contrast images (f, g) showing that the disks are uniformly constructed by parallel granular rods with a cortex of organic and amorphous  $\text{CaCO}_3$  components. (h) AFM amplitude imaging of the rod grains with traces of the cortex.



Periostracal calcifications were previously described and illustrated in oysters, the shells of which are composed of a single polymorph: calcite. Yamaguchi [28] has observed that “the shell margin is soft and flexible because the growing crystals on the periostracum are distinct from each other.... The growing shell margin is so soft that the periostracal sheet together with its spherulites is rolled into the shell when the mantle margin is withdrawn”. More recently, Checa *et al.* [29] have described a similar processus in *Neotrigonia*, a bivalve shell composed of a nacreous layer and an aragonite prismatic layer. The “calcified bosses” [29] or “knob (= mamelon)” [30] are clearly visible at the outer surface of the shell and, from a microstructural point of view are “fully continuous” with the prisms [29]. Nevertheless, distribution maps show a change in the chemical composition [30].

In practice, the completed disks are driven to the correct position to be incorporated into the shell as the forefront units of the prismatic layer (Figure 8e: arrows) through an approximately  $180^\circ$  rocking motion around an axis parallel to shell margin. This movement enables the outer side of the disks to be aligned with previous shell surface, thereby increasing shell length. Concomitantly, the inner surface of the newly positioned disks is now involved in the layered growth mode, which then enables the thickness of the shell to increase.

### 3.2. Insertion of the New Forefront Shell Units into the Common Mineralization Mode of the Mantle Epithelium

The transition from disk to prism stages is a crucial step in the formation of shell microstructure. Data from Figures 5 and 6 illustrate the two distinct processes to be considered at this point of shell ontogeny: determinism of prism morphology (Section 3.2.1) and origin of crystallographic orientation (Section 3.2.2).

### 3.2.1. Origin of Prism Morphology

In accordance with the reported opinions of Wada, Wilbur, Taylor and Kennedy, Checa *et al.* [24] admit that a direct crystallization allows explaining the polygonal morphology of the prisms. Polygonal organization of the calcite is generally attributed to physical mechanisms. For example, Taylor and Kennedy [9] supported the crystallization model proposed by Voll [31] concerning organization of the sedimentary grains: “when three boundaries meet at a common edge, the triangle of forces produces an interfacial angle of 120°; the usual shape arising by this process is an irregular pentagon”. Following a purely theoretical approach, Ubukata [32,33] also developed a model of crystallization based on variation of nucleation potential in order to explain the diversity of polygonal patterns within a single shell. Data reported here suggest a challenging view to the “crystal growth competition concept” (CGC) proposed by Checa *et al.* [34,35] as the determinant factor for the morphology of the calcite prisms and other types of microstructures.

No polygonal network (or “envelope”) was visible around the disks (Figure 4) whereas polygonal network appears immediately after the rocking movement of the disks (Figure 8e), when begins the layered growth mode that ensures thickening of the shell (Figure 5). In most cases a direct correspondence exists between a given disk and the underlying prism (Figure 5c,d) but examples of envelopes surrounding two or sometimes three irregular disks can be observed (Figure 5h). This discrepancy is related to the stepping elongation of the shell (Figure 3a–d). Observing the concentric units produced during a shell elongation step (Figure 3a–e) it is clear that the structural units produced at the end of the elongation cycle are smaller than those produced at its beginning. Figure 3f emphasizes this size difference by showing the contact between the end of an elongation cycle and the early disks produced by the next one. Capability of the polygonal envelopes to include two or three of these small and irregular units regularizes the prismatic structure of the shell.

Remarkably, the developmental sequence of the *Pinctada* prisms allows significant observation casting doubt about an overall validity of the crystal growth competition concept. According to CGC, prisms whose *c* crystallographic axes are oriented perpendicular to shell plan are favored in the competition and progressively eliminate the misoriented neighboring prisms. Such a mechanism leads to an increase of the mean diameter of the prisms. Therefore splitting of a well established monocrystalline unit into several subunits, each of them continuing to grow with its own crystallographic orientation, is basically opposing the concept of competition. Splitting of the *Pinctada* prisms is long known (Figure 1c in [36], plate 1) and further investigations have been carried out showing that splitting of the crystal-like mineral in the prisms is correlated to appearance of an organic subdivision of the initial prismatic compartment.

Worth to note that such an unforeseen splitting process appears more understandable in the layered growth and crystallization model (LGC) [15]. As seen by Figure 6f (see also contribution of synchrotron based mapping [16]), the newly formed layers incorporate the structural changes resulting from secretion of the molecules forming the internal subdivisions of the prisms. Such a synchronic microstructural transformation observed in the prismatic layer of the *Pinctada* exemplifies and brings substantial support to the concept of time-based functional changes in the mineralizing cells generated in the outer grove of the mantle, as hypothesized by Taylor and Kennedy [9] and Griffin [26].

### 3.2.2. Origin of Crystallographic Orientation of the Prisms

Although an overall similarity in crystallographic orientation of the calcite prisms has long been noticed ( $c$  axis globally perpendicular to shell surface) [2], no explanation has been proposed regarding origin of this specificity. Explanation generally taken into account is that  $c$  axis is the most favorable to prism elongation. Worth to note that nacreous tablets provide a counter example (nacreous tablets are flattened perpendicular to their  $c$  axis which is the preferential growth direction of chemical aragonite fibers) casting doubt about explanation transferred from mineral chemistry to biomineralization domain.

Evidence of the single crystal-like status of discoid stages predating formation of the prisms (Figure 4e–i) and AFM investigation showing the consistent orientation of mineral rods within a given disk (Figure 9d–h) lead to suggest that crystallographic status of the *Pinctada* prisms is inherited from the overlying disks. The organic rings, first observed by Mikkelsen *et al.* [10] on the outer surface of the shell margin, are significant vestiges of the passage from disk to prism stage in the formation of the *Pinctada* shell outer layer. Consistency of the polarization colors between inner- and outer-ring mineral domains of a given prism (Figure 5d) show that, after having been positioned to their final place at the shell margin, single-crystal like disks are acting as templates for the early step of prism crystallization when, owing to the change in disks position, the layered growth process is substituted to the concentric disk growth mode.

Unfortunately no physical evidence presently exists explaining how these disk central nodules (Figure 9a, arrows) may act as crystallization centers, triggering deposition of the consistently oriented calcite rods (Figure 9d–g). Once again, similarity between these ultrastructural data and various others mostly concerning nacre ultrastructure, from the Mutvei's pictures of nacre ultrastructure [37] to Nudelman's biochemical characterization of the initial center of nacreous tablets [22] deserves to be reminded. It emphasizes the role of organic precursors in the formation of these complex microstructural units. That comparable nanoscale patterns can be found at the origin of calcite and aragonite ultrastructures also suggests that both Ca-carbonate polymorphs could be used and controlled by rather equivalent mechanisms.

### 3.3. Perturbation of the Mineralizing Mechanism Predating Nacre Deposition at the End of Prism Growth: An Additional Example of Time-Based Metabolic Change in Aging Cells

From concentric crystallization of the periostracal disks to splitting of the calcite prisms, a constructive sequence of events contributes to create the specific structural pattern of the prisms that form the outer shell layer in *Pinctada margaritifera*. This species is remarkable by the thickness of its internal layer made of nacre (aragonite tablets). A primary observation suggests that lateral expansion of the nacreous layer resulting in coverage of the prismatic internal surface causes cessation of prism growth (Figures 1b and 2a, arrows).

Contrastingly, the converging structural and biochemical evidences gathered in Figure 7 establish that the actual cause of the end of prism growth is internal: the last event in the biochemical sequence driving prism development. Progressive reduction of growth layer thickness and mineral deposition on restricted areas resulting in dome-shaped prism ends (Figure 7c,g,l), form obvious indications of regressive mineralization capability. From a biochemical viewpoint changes in composition of the

mineralizing phase, assessed by synchrotron based mapping (Figure 7i,j) are correlated to this regression of secretory mechanism. Supporting interpretation of an internal (*i.e.*, genomic) origin of the end of prism growth, formation of a biochemically specific coverage membrane [17] (Figure 7h) represent additional symptom of the important metabolic changes occurring in the mineralizing cell layer.

That all these converging indications were obtained from prismatic structures not covered yet by the earliest deposition of the nacreous layer unambiguously establishes that cessation of the growth of calcite prisms results from metabolic evolution, taking place as a specific step in the programmed evolution of gene expressions controlling formation of the prismatic structures all along the animal life.

## 4 Material and Methods

### 4.1. Materials

Shells involved in this study have been grown at the Institut français de recherche pour l'exploitation de la mer (IFREMER) hatchery of Vairao (Tahiti, Polynesia) and the relevant marine areas. Juvenile specimens were produced and grown at the hatchery, whereas pearl oysters were grafted and grown at the Polynesian Grafting School of the Rangiroa lagoon. Most of the studied materials were produced during the Adequa groupement de recherche research program with financial support from the Polynesian Ministère des Ressources Marines.

### 4.2. Methods

Optical microscopy included observation by transmitted light (natural and crossed-polarized) using reflected natural light, UV epi-fluorescence by mercury lamp light filtered by UV (365 nm) and blue (435 nm) filters using Zeiss Standard Universal epi-illumination.

Secondary Electron Microscopy (SEM) observations were carried out using a Philips XL30 (Philips, Eindhoven, The Netherlands) equipped with a secondary electron and backscattered electron (BSE) detectors and a PHENOM PRO X microscope (Phenom-World, Eindhoven, The Netherlands) (only BSE). In this technique, imaging contrast is due to the difference in BSE ratio, which depends on the atomic number of the atoms composing the substrate material.

Micro-XANES biochemical mapping (X-ray Absorption Near Edge Structure spectroscopy) was carried out at the ID21 beamline of the European Synchrotron Radiation Facility. The ID21 Scanning X-ray Microscope uses Fresnel zone plates as focusing optics to generate a submicron X-ray probe. An energy range between 2 and 7 keV is available, which provides access to both the sulphur K-edge at 2472 eV (sulfur in amino acids) and 2482.5 eV (sulfated sulfur in polysaccharides).

Microbeam X-ray Bragg diffraction was carried out at the European Synchrotron Radiation Facility at the ID13 beamline. Using a set of refractive silicon lenses, the 14.9 keV monochromatic beam was focused down to a 100 nm beam spot. The sample was placed vertically in the focal plane onto a piezoelectric stage mounted on the top of a hexapod. This set-up allows the precise positioning of the sample, whose region of interest is selected with the help of an optical microscope. Furthermore, the set-up permits the scanning of the crystal orientation (rocking curve) in order to bring the crystal lattice planes in Bragg diffraction conditions. The resulting Bragg diffraction peaks are measured by a Frelon

camera, located at 0.3 m from the sample, allowing the investigation of several diffraction peaks simultaneously.

Raman mapping was undertaken using a WITec alpha 300 R (WITec GmbH, Ulm, Germany) confocal Raman microscope [38]. Scans are obtained using a piezoelectric scanner table having a scan range of  $200\ \mu\text{m} \times 200\ \mu\text{m}$ , and a minimum step size of 4 nm lateral, and 0.5 nm vertical. Imaging was performed using a 488 nm wavelength laser and a dedicated ultra-high throughput spectrometer (UHTS 300, WITec) (grating, 600/mm, 500 nm blaze). On an area of  $50\ \mu\text{m} \times 50\ \mu\text{m}$  on  $300 \times 300$  points, spectra were obtained at an integration time of 0.05 s per point.

For AFM observation, samples were polished using diamond paste and cleaned with milli-Q water (Merck Millipore, Molsheim, France). Samples were observed using a Veeco AFM Dimension 3100 Nanoscope III (Veeco, Plainview, NY, USA). The probe consists of a cantilever with an integrated silicon tip. Samples were imaged at room temperature and in air using tapping mode phase contrast imaging.

## 5. Conclusions

(1) Four developmental stages have been recognized in the columnar prisms of calcite in *Pinctada margaritifera*;

(2) Initial crystallization occurs as round-shaped flattened disks, with single crystal-like behavior, formed between the inner side of the periostracum and the cell layer of the outer periostracal groove of the mantle;

(3) Formation of prisms occurs when the developed disks are positioned in the shell plan, forming the forefront units of the shell. Concomitantly, disks are involved in the common layered-mode of mineralization. This stepping-growth process involves both deposition of the mineralized phase and formation of the “honeycomb” organic envelopes;

(4) The next structural stage results from splitting of the single crystal-like prism, due to formation of distinct compartments within the polygonal envelopes. Prism subunits are separated by condensed organic compounds forming irregular laminae;

(5) Such a regular sequence of mineralizing events indicates that both morphological and structural patterns of the prisms (including crystallization of the mineralized components) are submitted to a permanent biological control, from their early developmental stages to end of their growth;

(6) Progressive modification of the mineralizing matrices, involving both polygonal envelopes and inner crystallized phases, reveals that end of prism growth predates deposition of the first aragonitic components of the inner shell layer, establishing that lateral expansion of nacre is not the cause of the interruption of prism growth.

## Acknowledgements

This work has been supported by ANR grant to the 3D-PtyCCoBio project (11-BS10-005-02) and by ESRF allowance of beam time at ID13 and ID21 (CH1569, EC24 and SC3550 sessions). Authors acknowledge contribution of Dr. C.T. Williams (NHM London) for both manuscript comment and language checking, and S. Piazzolo (now Macquarie University, Australia) for communication of an EBSD data.

## Author Contributions

This paper was initiated by J.P. Cuif and Y. Dauphin. Contributions from other co-authors were incorporated in final text including those based on Raman mapping (G. Nehrke) and EBSD (A. Perez-Huerta). G. Le Moullac is in charge of the IFREMER *Pinctada* hatchery at the Taravao biological Station (Tahiti). M. Burghammer, V. Chamard and P. Godard carried out micro-diffraction experiments at the ESRF Grenoble (ID 13 beam line) and interpreted the results.

## Conflicts of Interest

The authors declare no conflict of interest.

## References

1. Watabe, S.; Maeyama, K.; Nagasawa, H. *Recent Advances in Pearl Research—Proceedings of the International Symposium on Pearl Research 2011*; TerraPub: Tokyo, Japan, 2013, p. 276.
2. Schmidt, W.J. *Die Bausteine des Tierkörpers in Polarisierendem Lichte*; Cohen Verlag: Bonn, Germany, 1924; p. 528. (In German)
3. Bøggild, O.B. The shell structure of the molluscs. *K. Dan. Vidensk. Selsk. Skr. Naturvidensk. Math. Afd.* **1930**, *9*, 231–326.
4. Taylor, J.D.; Kennedy, W.J.; Hall, A. The Shell Structure and Mineralogy of the Bivalvia: I. Introduction. Nuculacae-Trigonacae. *Bull. Br. Mus. Zool.* **1969**, *3*, 1–125.
5. Taylor, J.D.; Kennedy, W.J.; Hall, A. The Shell Structure and Mineralogy of the Bivalvia: II. Lucinacea-Clavagellacea, Conclusions. *Bull. Br. Mus. Zool.* **1973**, *22*, 253–294.
6. Carter, J.G. Evolutionary significance of shell microstructures in the Palaeotaxodonta, Pteriomorpha and Isofilibranchia (Bivalvia: Mollusca). In *Skeletal Biomineralization: Patterns, Processes and Evolutionary Trends*; Carter, J.G., Ed.; Van Nostrand Reinhold: New York, NY, USA, 1990; Volume 1, pp. 135–296.
7. Wilbur, K.M. Shell formation and regeneration. In *Physiology of Mollusca*; Wilbur, K.M., Owen, G., Eds.; Academic Press: New York, NY, USA, 1964; Volume 1, pp. 243–282.
8. Wada, K. Crystal growth of molluscan shells. *Bull. Natl. Pearl Res. Lab.* **1961**, *36*, 703–828.
9. Taylor, J.D.; Kennedy, W.J. The influence of the periostracum on the shell structure of bivalve Molluscs. *Calcif. Tissue Res.* **1969**, *3*, 274–283.
10. Mikkelsen, P.M.; Tëmkin, I.; Bieler, R.; Lyons, W.G. *Pinctada longisquamosa* (Dunker, 1852) (Bivalvia: Pteriidae), an unrecognized pearl oyster in the Western Atlantic. *Malacologia* **2004**, *46*, 473–501.
11. Saleuddin, A.S.M.; Petit, H. The mode of formation and the structure of the periostracum. In *The Mollusca*; Saleuddin, A.S.M., Wilbur, K.M., Eds.; Academic Press: New York, NY, USA, 1983; Volume 4, pp. 199–234.
12. Soldati, A.L.; Jacob, D.E.; Wehrmeister, U.; Hofmeister, W. Structural characterization and chemical composition of aragonite and vaterite in freshwater cultured pearls. *Mineral. Mag.* **2008**, *72*, 577–590.

13. Volkmer, D. Biologically inspired crystallization of calcium carbonate beneath monolayers: A critical overview. In *Handbook of Biomineralization: Biomimetic and Bioinspired Chemistry*; Behrens, P., Baeuerlein, E., Eds.; Wiley: Hoboken, NJ, USA, 2007; pp. 65–87.
14. Marsh, M.E.; Sass, R.L. Calcium-binding phosphoprotein particles in the extrapallial fluid and innermost shell lamella of clams. *J. Exp. Zool.* **1983**, *226*, 193–203.
15. Cuif, J.P.; Dauphin, Y.; Nehrke, G.; Nouet, J.; Perez-Huerta, A. Layered growth and crystallization in calcareous biominerals: Impact of structural and chemical evidence on two major concepts in invertebrate biomineralization studies. *Minerals* **2012**, *2*, 11–39.
16. Dauphin, Y.; Cuif, J.P.; Doucet, J.; Salomé, M.; Susini, J.; Williams, C.T. *In situ* chemical speciation of sulfur in calcitic biominerals and the simple prism concept. *J. Struct. Biol.* **2003**, *142*, 272–280.
17. Farre, B.; Brunelle, A.; Laprévotte, O.; Cuif, J.P.; Williams, C.T.; Dauphin, Y. Shell layers of the black-lip pearl oyster *Pinctada margaritifera*: Matching microstructure and composition. *Comp. Biochem. Physiol.* **2011**, *159*, 131–139.
18. Carter, J.G.; Aller, R.C. Calcification in the bivalve periostracum. *Lethaia* **1975**, *8*, 315–320.
19. Carter, J.G. *Ecology and Evolution of the Gastrochaenacea (Mollusca, Bivalvia) with Notes on the Evolution of the Endolithic Habitat*; Peabody Museum of Natural History: New Haven, CT, USA, 1976; pp. 1–92.
20. Jabbour-Zahab, J.; Chagot, D.; Blanc, F.; Grizel, H. Mantle histology, histochemistry and ultrastructure of the pearl oyster *Pinctada margaritifera* (L.). *Aquat. Living Res.* **1992**, *5*, 287–298.
21. Suzuki, M.; Nakayama, S.; Nagasawa, H.; Kogure, T. Initial formation of calcite crystals in the thin prismatic layer with the periostracum of *Pinctada fucata*. *Micron* **2013**, *45*, 136–139.
22. Nudelman, F.; Gotliv, B.A.; Addadi, L.; Weiner, S. Mollusk shell formation: mapping the distribution of organic matrix components underlying a single aragonitic tablet in nacre. *J. Struct. Biol.* **2006**, *153*, 176–187.
23. Dauphin, Y. Nanostructures de la nacre des tests de céphalopodes actuels. *Paläontol. Z.* **2001**, *75*, 113–122. (In French)
24. Checa, A.G.; Bonarski, J.T.; Willinger, M.G.; Faryna, M.; Berent, K.; Kania, B.; Gonzalez-Segura, A.; Pina, C.M.; Morawiec, J.P.A. Crystallographic orientation inhomogeneity and crystal splitting in biogenic calcite. *J. R. Soc. Interface* **2013**, *10*, 20130425.
25. Cuif, J.P.; Dauphin, Y.; Sorauf, J.E. *Biominerals and Fossils through Time*; Cambridge University Press: Cambridge, UK, 2011; p. 490.
26. Griffin, L.E. *The Anatomy of the Nautilus Pompilius*; Johns Hopkins Press: Baltimore, MD, USA, 1900; pp. 101–197.
27. Chu, P.K.; Li, L. Characterization of amorphous and nanocrystalline carbon films. *Mater. Chem. Phys.* **2006**, *96*, 253–277.
28. Yamaguchi, K. Shell structure and behaviour related to cementation in oysters. *Mar. Biol.* **1994**, *118*, 89–100.
29. Checa, A.G.; Salas, C.; Harper, E.M.; de Dios Bueno-Perez, J. Early stage biomineralization in the periostracum of the “living fossil” bivalve *Neotrigonia*. *PLoS One* **2014**, *9*, e90033.
30. Dauphin, Y.; Cuif, J.P.; Salomé, M. Structure and composition of the aragonitic shell of a living fossil: *Neotrigonia* (Mollusca, Bivalvia). *Eur. J. Mineral.* **2014**, *26*, 485–494.

31. Voll, G. New work on petrofabrics. *Geol. J.* **1961**, *2*, 503–567.
32. Ubukata, T. Architectural constraints on the morphogenesis of prismatic structures in Bivalvia. *Palaeontology* **1994**, *37*, 241–261.
33. Ubukata, T. Nucleation and growth of crystals and formation of cellular pattern of prismatic shell microstructure in Bivalve Molluscs. *Forma* **2001**, *16*, 141–154.
34. Checa, A.G.; Rodríguez-Navarro, A.B.; Esteban-Delgado, F.J. The nature and formation of calcitic columnar prismatic shell layers in pteriomorphian bivalves. *Biomaterials* **2005**, *26*, 6404–6414.
35. Checa, A.G.; Okamoto, T.; Ramírez, J. Organization pattern of nacre in Pteriidae (Bivalvia: Mollusca) explained by crystal competition. *Proc. Biol. Sci.* **2006**, *273*, 1329–1337.
36. Dauphin, Y.; Kervadec, G. Comparaison des diagenèses subies par les phases minérale et protéique soluble des tests de Mollusques Céphalopodes Coléoides. *Palaeontographica* **1994**, *A232*, 85–98. (In French)
37. Mutvei, H. Ultrastructure of the mineral and organic components of molluscan nacreous layers. *Biomineralization* **1970**, *2*, 48–72.
38. Nehrke, G.; Nouet, J. Confocal Raman microscope mapping as a tool to describe different mineral and organic phases at high spatial resolution within marine biogenic carbonates: Case study on *Nerita undata* (Gastropoda, Neritopsina). *Biogeosciences* **2011**, *8*, 3761–3769.

© 2014 by the authors; licensee MDPI, Basel, Switzerland. This article is an open access article distributed under the terms and conditions of the Creative Commons Attribution license (<http://creativecommons.org/licenses/by/4.0/>).